ISSN 0020-4412, Instruments and Experimental Techniques, 2023, Vol. 66, No. 2, pp. 350–357. © Pleiades Publishing, Ltd., 2023.

LABORATORY TECHNIQUES

Large-Bandwidth High-Gain Low-Noise Transimpedance Amplifier for Scanning Tunneling Microscope

Ying-Xin Liang[a,*]

[a] *Anyang Normal Univ, Sch Phys & Elect Engn, Anyang, Henan, 455000 China*

**e-mail: cryoliang@qq.com*

Received July 9, 2022; revised September 1, 2022; accepted November 21, 2022

Abstract—In this work, a design of large-bandwidth high-gain low-noise transimpedance amplifier (TIA) for scanning tunneling microscope (STM) is proposed. The simulations show that the proposed TIA has the bandwidth higher than 200 kHz, two orders of magnitude higher than those of conventional commercial TIAs for STM. At low frequencies, the noises of the proposed TIA are almost the same as the conventional commercial ones with the same transimpedance gain. At high frequencies, its calculated input equivalent noise voltage power spectral density (PSD) is 40 nV^2/Hz and its input equivalent noise current PSD is 3.2 fA^2/Hz at 10 kHz. The corresponding values are 23 nV^2/Hz and 88 fA^2/Hz at 100 kHz. The STM with the proposed TIA can meet the needs of fast high-quaility STM imaging measurements and fast high-energy-resolution scanning tunneling spectra measurements for the low-conducting materials, such as complex organic systems and wide bandgap semiconductors.

DOI: 10.1134/S0020441223020264

1. INTRODUCTION

High performance transimpedance amplifier (TIA) is a key element in scanning tunneling microscopy/spectroscopy [1, 2]. For the application of scanning tunneling microscopy (STM) to investigate complex organic systems, such as biological macromolecules (DNA [3], RNA [4–6], and proteins [7], etc.) and membranes [8], one of the main problems is the ability for the biological samples to sustain only an extremely low current [9]. Furthermore, for many biological samples, due to their variability, the real-time observation is required, so fast STM imaging measurements with high-quaility and fast scanning tunneling spectroscopy (STS) measurements with high-energy-resolution are necessary. For the application of STM to investigate low-conductivity semiconductor materials, such as wide bandgap semiconductors, the tunnel current is typically less than 100 pA [10]. In semiconductor industry, the fast high-quaility STM imaging measurements and fast high-energy-resolution STS measurements for quality tests of wide bandgap semiconductors are urgently needed to meet the high production efficiency. For the conventional TIA in STM with the gain higher than 1 GV/A the typical bandwidth is less than 1 kHz [1, 11], which is too low for fast imaging measurements and fast STS measurements. Therefore, the STM with the conventional TIA [11] is not suitable for these measurements.

In this work, a TIA for STM with transimpedance gain of 10 GV/A and bandwidth larger than 200 kHz is proposed. Its transient response time is only 3.5 μs. Its equivalent input noise voltage PSD is only 23 nV^2/Hz in f >100 kHz. Its equivalentinput noise current PSD is only 4.7 fA^2/Hz at 10 kHz, and 88 fA^2/Hz at 100 kHz. For the various low-conductivity materials, fast high-quaility STM imaging measurements and fast high-energy-resolution STS measurements can be performed with this apparatus.

2. DESIGN OF STM-TIA AND ITS ELECTRICAL PERFORMANCES

Figure 1 shows the circuit of the proposed TIA. It consists of several components: the pre-amplifier (Pre-Amp) shown in dashed box (A_1) of Fig. 1 and the post-amplifier (Post-Amp) shown in dashed box (A_2), the compensated feedback network shown in dashed box (B). The two stage amplifier made of the Pre-Amp and Post-Amp is called as inverting amplifier (Inv-Amp). The Inv-Amp is connected with the feedback network to form TIA. The circuit shown in dashed box (C) of Fig. 1 is called as signal source circuit. The TIA is connected with the signal source circuit to form STM-TIA. The parameters of all components of the STM-TIA circuit are listed in Table 1.

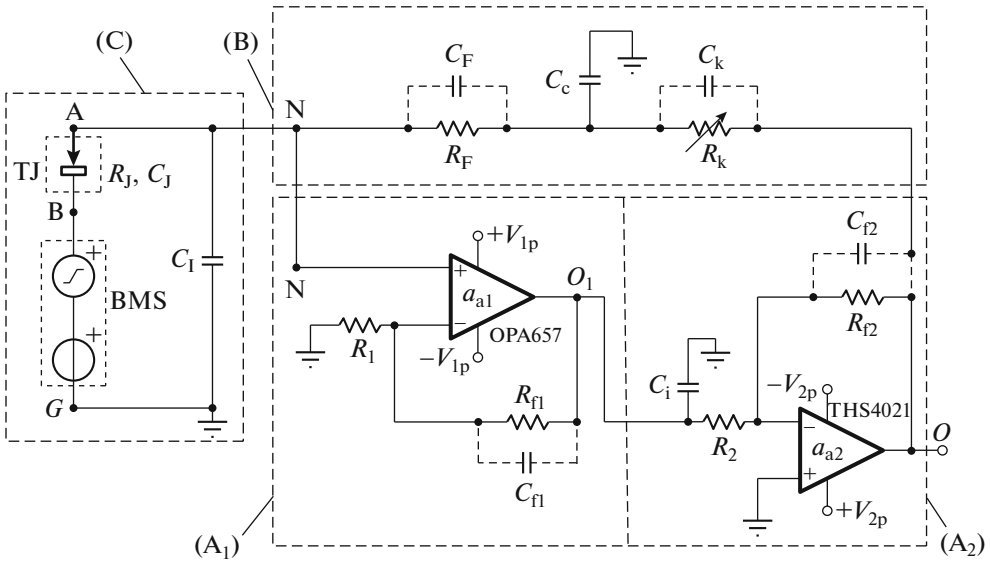

Fig. 1. STM-TIA circuit. Pre-Amp is shown in dashed box (A_1), Post-Amp—in dashed box (A_2), the compensated feedback network—in dashed box (B), the signal source circuit—in dashed box (C).

2.1. Design of Pre-Amp

The Pre-Amp is a noninverting amplifier consisting of a commercial operational amplifier (OPA) OPA657 [12] and two resistors R_{f1} and R_1 [13]. C_{f1} is the parasitic capacitance of R_{f1}. The loop gain of the Pre-Amp is $T_{L1}(f) = a_{a1}(f)\beta_1(f)$, where $a_{a1}(f)$ is the open-loop voltage gain of OPA657 and $\beta_1(f)$ is the feedback factor of the noninverting amplifier; $a_{a1}(f) \approx a_{a10}/(1 + jf/f_{1b})$ and $\beta_1(f) \approx 1\Big/\left[1+\dfrac{R_{f1}}{R_1(1+j2\pi fC_{f1})}+R_{f1}\dfrac{j2\pi f(C_{1c}+C_1)}{1+j2\pi fR_{f1}C_{f1}}\right]$. Here, a_{a10} is the open-loop voltage gain of OPA657 for $f\to 0$, f_{1b} is the upper cut-off frequency of OPA657, C_{1c} is the common-mode input capacitance of OPA657, C_1 is its differential input capacitance, and R_{1a} is the input resistance of OPA657.

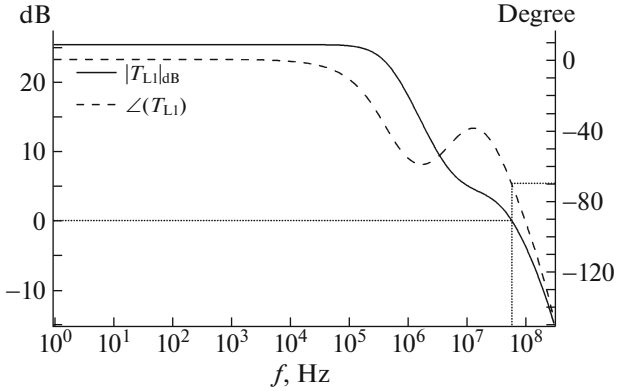

Fig. 2. TINA-TI simulation results for the loop gain of Pre-Amp $T_{L1}(f)$. As $|T_{L1}(f)|_{dB} > 0$ dB, $\angle(T_{L1}(f)) > -70°$.

$T_{L1}(f)$ is simulated by TINA-TI [14], and the simulation results are shown in Fig. 2. At f_1 where the moudulus $|T_{L1}(f_1)|_{dB} = 0$ dB, the argument $\angle(T_{L1}(f_1)) = -82°$, namely its phase margin of stability of the Pre-Amp is 98°. $|T_{L1}(f)|_{dB}$ decreases monotonously with the increase of f, so its gain margin of stability is much greater than 6 dB. The voltage gain of the Pre-Amp is

$$A_{v1}(f) \approx \frac{R_{f1}}{R_1}\frac{1}{1+R_{f1}/(a_{a1}R_1)+j2\pi fR_{f1}C_{f1}}. \qquad (1)$$

$|A_{v1}(f)|_{dB}$ and $\angle(A_{v1}(f))$ are simulated by TINA-TI, (see Fig. 3), $A_{v1}(f)$ is identical with the calculated value obtained with Eq. (1). Figure 3 shows that the upper cut-off frequency (3 dB drop of frequency) for $A_{v1}(f)$, is $f_{h1} = 3.56$ MHz, and $\angle(A_{v1}(f_{h1})) = 43.6°$. There is no "gain peaking" on the curve of $|A_{v1}(f)|_{dB}$, so the stability of the circuit is verified [13].

2.2. Design of Post-Amp

The Post-Amp is an inverting amplifier consisting of a commercial OPATHS4021 [15] and two resistors R_{f2} and R_2 [13]. C_{f2} is the parasitic capacitance of R_{f2}. The loop gain of the Post-Amp is $T_{L2}(f) = a_{a2}(f)\beta_2(f)$, where $a_{a2}(f)$ is the open-loop voltage gain of THS4021 and $\beta_2(f)$ is the feedback factor of the inverting amplifier; $a_{a2}(f) \approx a_{a20}/(1 + jf/f_{2b})$ and $\beta_2(f) \approx 1\Big/\left[1+\dfrac{R_{f2}}{R_2(1+j2\pi fC_{f2})}+R_{f2}\dfrac{j2\pi fC_2}{1+j2\pi fR_{f2}C_{f2}}\right]$. Here, a_{a20} is the open-loop voltage gain of THS4021 for $f\to 0$, f_{2b} is the upper cut-off frequency of THS4021, C_2 is the input capacitance of THS4021, and R_{2a} is the input resistance of THS4021.

$T_{L2}(f)$ is simulated by TINA-TI, and the simulation results are shown in Fig. 4. At f_2 where the moudulus $|T_{L1}(f_2)|_{dB} = 0$ dB, the argument $\angle(T_{L2}(f_2)) = -64°$, namely the phase margin of stability of the Post-Amp is 116°. $|T_{L2}(f)|_{dB}$ decreases monotonously with the increase of f, so its gain margin of stability is muchg reater than 6 dB. The voltage gain of the Post-Amp is

$$A_{v2}(f) \approx -\frac{R_{f2}}{R_2}\frac{1}{1 + R_{f2}/(a_{a2}R_2) + j2\pi f R_{f2}C_{f2}}. \quad (2)$$

$|A_{v2}(f)|_{dB}$ and $\angle(A_{v2}(f))$ shown in Fig. 5 are simulated by TINA-TI; $A_{v2}(f)$ is identical with the calculated results obtained with Eq. (2). As shown in Fig. 5, the upper cut-off frequency for $A_{v2}(f)$ is $f_{h2} = 2.12$ MHz and $\angle(A_{v2}(f_{h2})) = 134°$. There is no "gain peaking" on the curve of $|A_{v2}(f)|_{dB}$, so the stability of the circuit is verified [13].

2.3. Inv-Amp Performances

Cascade the Pre-Amp and Post-Amp to form the Inv-Amp. Both the Pre-Amp and Post-Amp are stable. The output resistance of the Pre-Amp is less than 10 Ω, and the input resistance of the Post-Amp is no less than 500 Ω. Therefore, the Inv-Amp is also stable. The open loop gain of the Inv-Amp is

$$a_A(f) = A_{v1}(f)A_{v2}(f). \quad (3)$$

Figure 6 shows the TINA-TI simulation results for the open loop gain of the Inv-Amp $a_A(f)$. The frequency corresponding to $\angle(a_A) = 135°$ is $f_{Inv} = 1.47$ MHz. There is no "gain peaking" on the curve of $|a_A(f)|_{dB}$, so the stability of the circuit is verified.

2.4. Frequency Compensition of Feedback Loop

The Inv-Amp is connected with the feedback network to form TIA. In order to increase the bandwidth of the TIA with the large freedback resistor R_F, frequency compensation must be used in the feedback loop, since the effect from the parasitic capacitance C_F of the freedback resistor R_F cannot be ignored at high frequencies. In Ref. [16], a very simple design of a feedback circuit with bandwidth compensation has been proposed. As shown in dashed box (B) in Fig. 1, taking $C_c \approx kC_F$, where $k = 10^4$, adjust $R_k \approx R_F/k$ to achieve $R_kC_c = R_FC_F$. Supposing the output voltage of the Inv-Amp is $\dot{v}$ and the current flowing through the feedback loop to the input N of the Inv-Amp is $\dot{i}_F$,

$$Z_F(f) = \frac{\dot{v}}{\dot{i}_F} \approx \frac{R_k + R_F}{1 + j2\pi f R_kC_k} \approx \frac{R_F}{1 + j2\pi f R_kC_k}. \quad (4)$$

In this work, $R_F = 10$ GΩ, $C_F \approx 0.3$ pF, $R_k \approx 1$ MΩ, and $C_k \approx 0.2$ pF, so that $f_F = 1/(2\pi R_kC_k)$ is about 800 kHz. In (0, 100 kHz) range, $|Z_F(f)| \approx R_F/|1 + j2\pi f R_kC_k|$ $> R_F$ is 1.008 and $|Z_F(f)| \le R_F$, so $Z_F(f)$ can be considered equal to R_F in (0, 100 kHz] range.

Table 1. Parameters of all components of CryoSTM-TIA circuit

Pre-Amp			
OPA657			
a_{a10}	75.6 dB	f_{1b}	480 kHz
C_{1c}	4.8 pF	C_1	0.7 pF
R_{1a}	10 TΩ	V_{1p}	5 V
$\overline{e_{1a}^2}$ ($f \ge 100$ kHz)	23 nV^2/Hz	$\overline{i_{1a}^2}$	1.7 fA^2/Hz
R_{f1}	150 kΩ	C_{f1}	~0.2 pF
R_1	500 Ω		
Post-Amp			
THS4021			
a_{a20}	97.5 dB	f_{2b}	14 kHz
C_2	1.5 pF	R_{2a}	5 MΩ
V_{2p}	15 V		
$\overline{e_{2a}^2}$ ($f \ge 10$ kHz)	2.25 nV^2/Hz	$\overline{i_{2a}^2}$ ($f \ge 10$ kHz)	4 pA^2/Hz
R_{f2}	150 kΩ	C_{f2}	~0.2 pF
R_2	500 Ω	C_i	50 pF
Feedback network			
R_F	10 GΩ	C_F	~0.3 pF
R_k	1 MΩ	C_k	~0.2 pF
C_c	3 nF		
Singal source circuit			
C_I	~0.5 pF		
R_J	≥10 MΩ	C_J	~10 fF

2.5. Circuit Stability of STM-TIA

The differential resistance of the tip-sample tunnel junction (TJ) in the signal source circuit is R_J, and its parallel capacitance is C_J. In this work, $R_J \ge 10$ MΩ, and C_J is usually of the order of fF [17]. BMS in Fig. 1 represents a voltage source, providing the applied DC bias and modulating signal voltage. C_I is the capacitance of the cable connecting the tip to the TIA input N. If the cable is 1cm long, the value of C_I is about 0.5 pF.

The loop gain of the STM-TIA (see Fig. 1) is

$$T_L(f) \approx a_A(f)\beta(f) = a_A(f)/[1/\beta(f)], \quad (5)$$

where, $\beta(f)$ is the feedback factor of the TIA, and its reciprocal is

$$1/\beta(f) = 1 + Z_F(f)(1/R_J + 1/R_A + j2\pi f C). \quad (6)$$

Here $Z_F(f) = R_F/(1+j2\pi f R_kC_k)$ and $C = C_A + C_I + C_J$. C_A is the input capacitance of the Inv-Amp, $C_A = C_{1c} +$

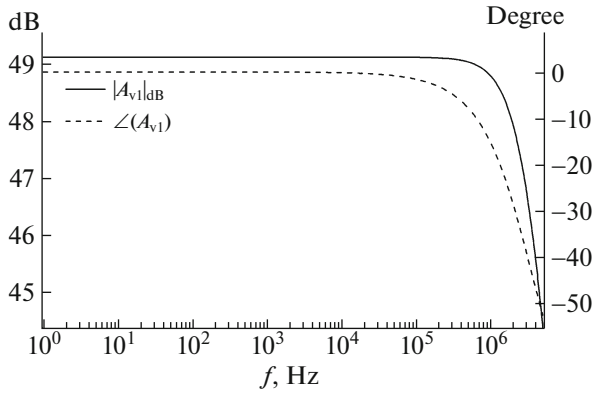

Fig. 3. TINA-TI simulation results for the gain of Pre-Amp $A_{v1}(f)$. The upper cut-off frequency for $A_{v1}(f)$ is f_{h1} = 3.56 MHz and $\angle(A_{v1}(f_{h1})) = 43.6°$. They are identical with the calculated results obtained with Eq. (1).

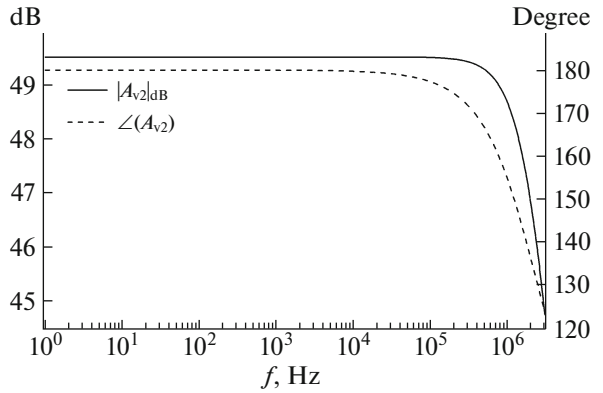

Fig. 5. TINA-TI simulation results for the gain of Post-Amp $A_{v2}(f)$. The upper cut-off frequency for $A_{v2}(f)$ is f_{h2} = 2.12 MHz and $\angle(A_{v2}(f_{h2})) = 134°$. They are identical with the calculated results obtained with Eq. (2).

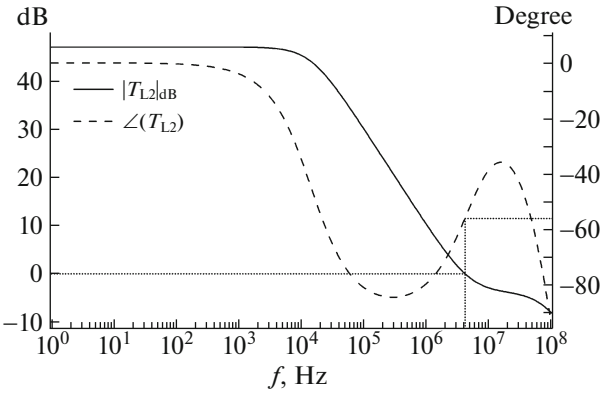

Fig. 4. TINA-TI simulation results for the loop gain $T_{L2}(f)$ of Post-Amp. As $|T_{L2}(f)|_{dB} > 0$ dB, $\angle(T_{L2}(f)) > -90°$.

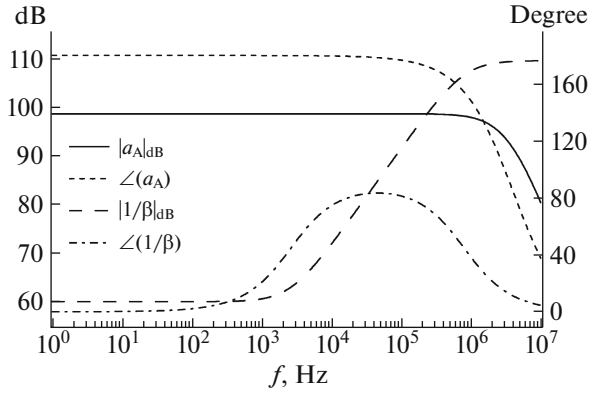

Fig. 6. TINA-TI simulation results for the open loop gain of Inv-Amp $a_A(f)$ and the calculated results for the reciprocal of the feedback factor of the TIA $1/\beta(f)$. The frequency for $\angle(a_A) = 135°$ is f_{Inv} = 1.47 MHz. The frequency for $|1/\beta|_{dB}$ qual to $|a_A|_{dB}$ is denoted as f_c = 235 kHz. $f_c << f_{Inv}$. $\angle(a_A(f_{Inv})) > 135°$ in $f < f_{Inv}$ and $\angle(1/\beta(f)) < 90°$. Therfore, as $|T_L(f)|_{dB} > 0$ dB, $\angle(T_L(f)) > -135°$.

$C_I = 5.5$ pF. R_A is the input resistance of the Inv-Amp, and $R_A = R_{Ia} = 10$ TΩ. $1/\beta(f)$ with $C_I = 0$ for $R_J = 10$ MΩ is calculated from Eq. (6), and the results are shown in Fig. 6. The frequency where $|1/\beta|_{dB}$ is equal to $|a_A|_{dB}$ is denoted as f_c = 235 kHz, and $f_c << f_{Inv}$; $\angle(1/\beta(f))$ is always smaller than 90°. Therefore, as $|T_L(f)|_{dB} > 0$ dB, $\angle(T_L(f)) > -135°$. Figure 7 shows the simulated moudulus $|T_L(f)|_{dB}$ and argument $\angle(T_L(f))$; as $|T_L(f)|_{dB} > 0$ dB, $\angle(T_L(f)) > -95°$. Since $|T_L(f)|_{dB}$ is monotone decreasing with the increase of f, the Inv-Amp circuit is stable [13]. The above conclusions for the circuit stability are still valid for $R_J > 10$ MΩ with $C_I \geq 0$ pF.

2.6. Transimpedance Gain of TIA

Applying a sinusoidal current source $\dot{i}_i$ in parallel with TJ, the generated output voltage of the STM-TIA is $\dot{v}_o$, and $A_i = \dot{v}_o/\dot{i}_i$ is called as the transimpedance gain of the STM-TIA. In (0, 300 kHz], A_i is

$$A_i = -\frac{Z_F}{1 - \frac{1}{a_A} - \frac{Z_F}{a_A R_A} - \frac{Z_F}{a_A R_J} - j2\pi f \frac{Z_F (C_A + C_I)}{a_A}}. \quad (7)$$

Disconnecting the TIA from the signal source circuit, and applying a sinusoidal current source $\dot{i}_{iT}$ into the input of the TIA, the output voltage is $\dot{v}_{oT}$, and $A_{iT} = \dot{v}_{oT}/\dot{i}_i$ is called as the transimpedance gain of the TIA. In (0, 300 kHz], A_i is

$$A_{iT} = -\frac{Z_F}{1 - \frac{1}{a_A} - \frac{Z_F}{a_A R_A} - j2\pi f \frac{Z_F C_A}{a_A}}. \quad (8)$$

Figure 8 shows the TINA-TI simulation results for $A_{iT}(f)/R_F$. There is no "gain peaking" on the curve of $|A_{iT}(f)/R_F|_{dB}$, so the stability of the circuit is verified. As shown in Fig. 8, the upper cut-off frequency for $A_{iT}(f)/R_F$ is f_{hT} = 216 kHz and $\angle(A_{iT}(f_{hT})/R_F) = 127°$. Therefore, for the proposed TIA, it is achieved high-gain and large-bandwidth. According to Eq. (7), with the increase of the cable length between the tip and the TIA input, i.e., the increase of C_I, the bandwidth for the STM-TIA is reduced. Therefore this cable should be as short as possible. Comparing Eq. (7) and Eq. (8), as $R_J \geq 0.001R_F$ and $C_I << C_A$, the upper cut-off frequency of the STM-TIA is apprxomitely equal to f_{hT}, so a high gain is achieved at large-bandwidth for the proposed STM-TIA.

2.7. Transient Response of STM-TIA

Figure 9 shows TINA-TI simulation results for the transient response performance of the STM-TIA with R_J = 10 GΩ. The dashed curve is the input up-step signal voltage V_{in}, and the solid curve is the response output voltage V_o. The time taken from adding the input step signal voltage to the output response is called transient response time t_r, and t_r < 3.5 μs as shown in Fig. 9. Furthermore, there are no "ringing" and "overshoot" characteristics on the output response curve, which also verifies the stability of the circuit.

3. NOISE PERFORMANCES OF STM-TIA

3.1. Equivalent Input Voltage Noise and Equivalent Input Current Noise of TIA

For the TIA, its equivalent input noise voltage is denoted as e_T, its equivalent input noise current is i_T, and their harmonic components of frequency f are E_T and I_T, respectively.

For the TIA, the circuit containing all noise sources is shown in Fig. 10. The equivalent input noise voltages of OPA657 for their two inputs are denoted as e_{1p} and e_{1n}, respectively, and their harmonic components of f are denoted as E_{1p} and E_{1n}, respectively. The equivalent input noise currents of OPA657 for their two inputs are denoted as i_{1p} and i_{1n}, respectively, and their harmonic components of f are denoted as I_{1p} and I_{1n}, respectively. The noise voltages of the resistor R_1 and the feedback resistor R_{f1} are denoted as e_1 and e_{f1} respectively, and the harmonic components of f are denoted as E_1 and E_{f1}, respectively. The equivalent input noise voltage of THS4021 is denoted as e_{2a}, and its harmonic component of f is denoted as E_{2a}. The equivalent input noise current of THS4021 is denoted as i_{2a}, and its harmonic component of f is denoted as I_{2a}. The noise voltages of the resistor R_2 and the feedback resistor R_{f2} are denoted as e_2 and e_{f2}, respectively, and their harmonic components of f are denoted as E_2 and E_{f2}, respectively. For the noise estimation, the

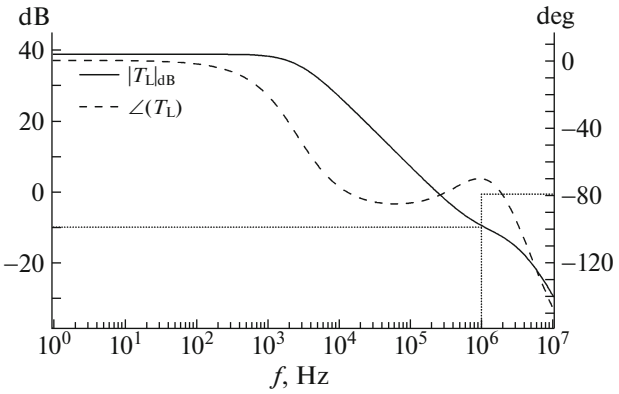

Fig. 7. TINA-TI simulation results for the loop gain $T_L(f)$ of STM-TIA with R_J = 1 MΩ. As $|T_L(f)|_{dB} > 0$ dB, $\angle(T_L(f)) > -95°$.

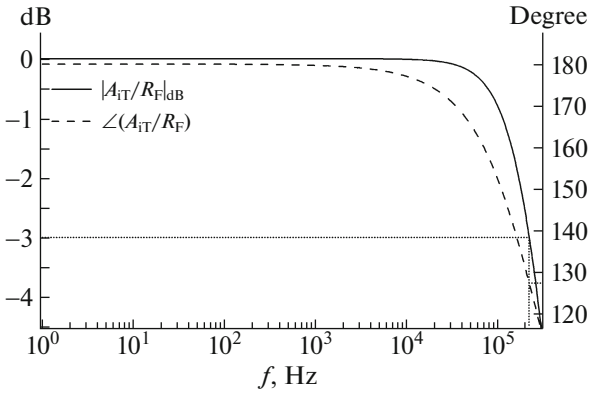

Fig. 8. TINA-TI simulation results for $A_{iT}(f)/R_F$, A_{iT} is the transimpedance gain of the TIA in the STM-TIA. $|A_{iT}(f_{hT})/R_F|_{dB} = -3$ dB and $\angle(A_{iT}(f_{hT})/R_F) = 127°$ at f_{hT} = 216 kHz.

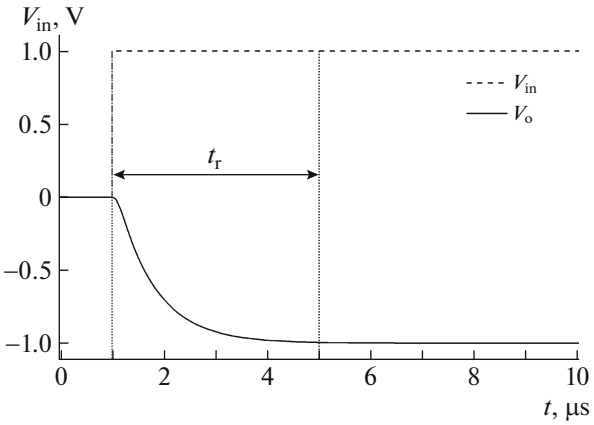

Fig. 9. TINA-TI simulation results for the transient response of the proposed STM-TIA. The dashed curve is the step input signal V_{in} and solid curve is the output response V_o. Transient response time is t_r < 3.5 μs. There is no ''ringing'' and ''overshoot''characteristics on the output response curve, verifying the circuit stability.

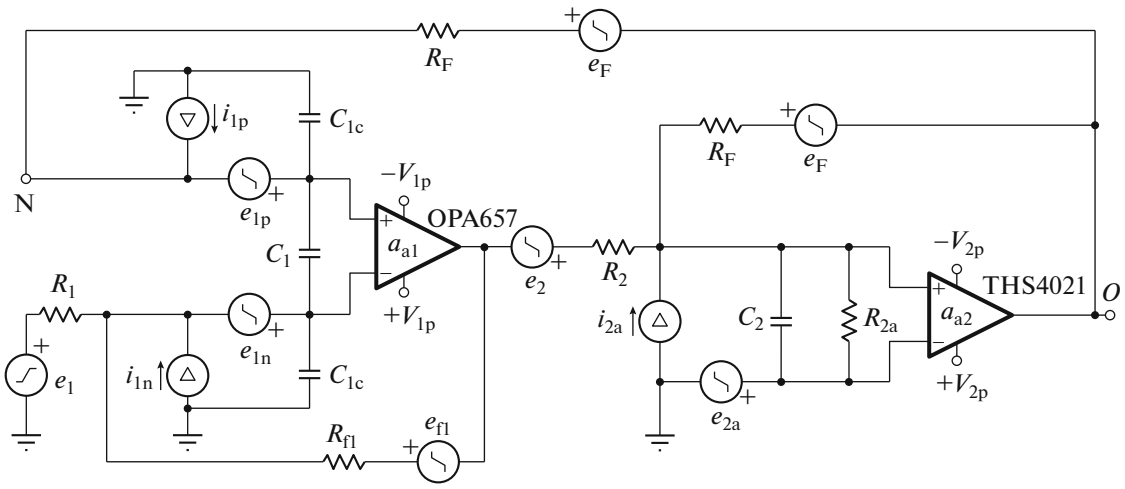

Fig. 10. Equivalent differential circuit of TIA containing all noise sources.

compensated feedback network in dashed box (B) of Fig. 1 can be simplified to a resistor of R_F. The noise voltage of R_F is denoted as e_F, and the harmonic components of f are denoted as E_F.

As input N is grounded, the output noise of the TIA is denoted as e_{ov}. The equivalent input noise voltage of the noiseless circuit of the TIA e_T as the input signal is added on input N, and the output noise is e_{ove}. For calculating e_T, the equation is established on $e_{ov} = e_{ove}$. Therefore, by the nodal analysis method:

$$E_T \approx E_{1p} - E_{1n} - I_{1n}R_1 - \frac{R_1}{R_{f1}}E_{fl} - E_1 - \frac{a_{a1}R_1 + R_{f1}}{R_{f1}}E_{2a} + \left(\frac{1}{a_{a1}} + \frac{R_1}{R_{f1}}\right)\left(E_2 + \frac{R_2}{R_{f2}}E_{f2} - E_{2a} + I_{2a}R_2\right). \quad (9)$$

As input N is open-circuit, the output noise of the TIA is denoted as e_{oi}. The equivalent input noise voltage of the noiseless circuit of the TIA i_T as the input signal is added on input N, and the output noise is e_{oie}. For calculating i_T, the equations are established on $e_{oi} = e_{oie}$. Therefore, by nodal analysis method,

$$I_T \approx i_{1p} - j2\pi f C_{1c}\left(E_{1p} - E_T\right) + \left(E_T + E_F\right)/R_F. \quad (10)$$

From $\begin{pmatrix} E_T E_T^* & E_T I_T^* \\ I_T E_T^* & I_T I_T^* \end{pmatrix}$, by Wiener–Khintchine theorem, $\begin{pmatrix} \overline{e_T^2} & \overline{e_T i_T^*} \\ \overline{i_T e_T^*} & \overline{i_T^2} \end{pmatrix}$ can be obtained [18, 19]. The small quantities in the Pre-Amp, such as the thermal noise of R_1 and R_{fl} can be ignored. All noises produced in the Post-Amp can also be ignored [19]. Therfore,

$$\overline{e_T^2} \approx \overline{e_{1p}^2} + \overline{e_{1n}^2} = \overline{e_{1a}^2}, \quad (11)$$

$$\overline{i_T^2} \approx \overline{i_{1p}^2} + (2\pi f)^2 C_{1c}^2 \overline{e_{1n}^2} + 4k_B T/R_F + \left(\overline{e_{1p}^2} + \overline{e_{1n}^2}\right)/R_F^2 = \overline{i_{1a}^2} + 2(\pi f)^2 C_{1c}^2 \overline{e_{1a}^2} + 4k_B T/R_F + \overline{e_{1a}^2}/R_F^2, \quad (12)$$

$$\overline{e_T i_T^*} = \overline{(i_T e_T^*)^*} \approx -j2\pi f C_{1c}\overline{e_{1n}^2} + \left(\overline{e_{1p}^2} + \overline{e_{1n}^2}\right)/R_F = -j\pi f C_{1c}\overline{e_{1a}^2} + \overline{e_{1a}^2}/R_F. \quad (13)$$

Here, $\overline{e_F^2} = 4k_B T R_F$ is the thermal noise of R_F, and it is only 1.6 fA²/Hz at room temperature. $\overline{e_{1p}^2} = \overline{e_{1n}^2} = \overline{e_{1a}^2}/2$ and $\overline{e_{1a}^2}$ is the announced equivalent input noise voltage PSD of OPA657, which is 40 nV²/Hz at $f =$ 1 kHz and 23 nV²/Hz in $f \geq$ 100 kHz [12]; $\overline{i_{1a}^2} = \overline{i_{1p}^2}$ and $\overline{i_{1a}^2}$ is the announced equivalent input noise current PSD of OPA657, which is only 1.7 fA²/Hz [12]. Therefore, $\overline{e_T^2}$ is 40 nV²/Hz and $\overline{i_T^2}$ is 3.2 fA²/Hz at 1 kHz, $\overline{e_T^2}$ is 40 nV²/Hz and $\overline{i_T^2}$ is 3.2 fA²/Hz at 10 kHz, and $\overline{e_T^2}$ is 23 nV²/Hz and $\overline{i_T^2}$ is 88 fA²/Hz at 100 kHz [12]. For FEMTO DE-DLPCA-200 with the gain of 1 GV/A, $\overline{e_T^2}$ is 16 nV²/Hz and $\overline{i_T^2}$ is 18.5 fA²/Hz at 1 kHz. For FEMTODE-LCA-200-10G with the gain of 10 GV/A, $\overline{e_T^2}$ is estimated as 81 nV²/Hz at 1 kHz and $\overline{i_T^2}$ is larger than 2.3 fA²/Hz at 1 kHz. The proposed TIA has the bandwidth higher than 100 kHz, and the noises of the proposed TIA are almost the same as the commercial ones with the same transimpedance gain at 1 kHz.

3.2. Inherent Noise of STM-TIA

The inherent noise of STM-TIA can be described by a virtual noise current source i_{in} in parallel with TJ,

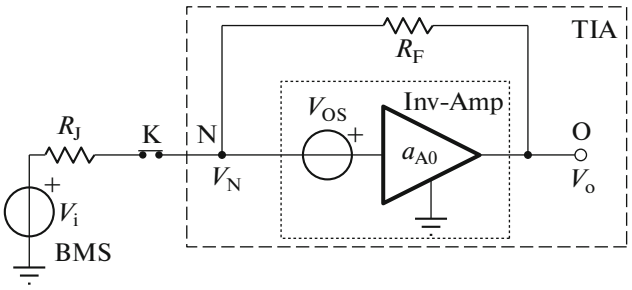

Fig. 11. DC circuit scheme for STM-TIA. The input offset voltage of Inv-Amp is denoted.

whose noise current PSD is called the equivalent input noise current PSD of STM-TIA, denoted as $\overline{i_{in}^2}$ or $\overline{i_{in}^2}(f)$. According to the noise model of the amplifier [19],

$$\overline{i_{in}^2} \approx \overline{i_T^2} + [1/R_J^2 + (2\pi f)^2 C_{IJ}^2]\overline{e_T^2} + (1/R_J + j2\pi f C_{IJ})\overline{e_T i_T^*} + (1/R_J - j2\pi f C_{IJ})\overline{i_T e_T^*}, \quad (14)$$

where $C_{IJ} = C_I + C_J$.

Putting Eqs. (11), (12), and (13) into Eq. (14),

$$\overline{i_{in}^2} \approx \overline{i_{1a}^2} + 2(\pi f)^2 (C^2 + C_{IJ}^2)\overline{e_{1a}^2} + 4k_B T/R_F + (1/R_F + 1/R_J)^2 \overline{e_{1a}^2}. \quad (15)$$

4. DC TUNNELLING CURRENT MEASUREMENT ACCURACY WITH THE PPOPOSED TIA IN STM

The Inv-Amp in the TIA has the input offset voltage V_{OS}, as shown in Fig. 11. It is easy to prove that $V_{OS} \approx V_{off}$, where V_{off} is the input offset voltage of OPA657. In Fig. 11, as switch K is open, for TIA, V_{OS} will cause a non-zero DC voltage V_{tia} at the output, and V_{tia} can be measured. It is also easy to prove that $V_{tia} \approx -V_{OS}$ [17]. As switch K is closed, the STM-TIA is formed. For the STM-TIA, applying the input voltage V_i, the potential at input N is V_N and at the output O the voltage is V_o which can be measured. The DC tunneling current is $I = (V_i - V_N)/R$, where R is TJ DC resistance corresponding to V_i. For the STM-TIA, $I = (V_N - V_o)/R_F$ and $V_o = a_{A0}(V_N + V_{OS})$.

$I_S = (V_{tia} - V_o)/R_F$ is the approximate value of the DC tunneling current I. For the STM-TIA, since $a_{A0} \approx -90000$, $|I - I_S|/|I|$ as the relative error for the DC tunneling current I is less than 12 ppm. The bias drop on TJ is $V = V_i - V_N = V_i - V_{tia} - (V_o - V_{tia})/(1 - a_{A0})$; as $R_J \geq 10$ MΩ, so $V_i - V_{tia}$ can be considered as the approximate value of V and the relative error is less than 1/89.

5. CONCLUSIONS

In this work, a large-bandwidth high-gain low-noise transimpedance amplifier (TIA) for STM is proposed to meet the needs of fast high-quaility STM imaging measurements and fast high-energy-resolution STS measurements for low-conductivity materials. For the noises of the proposed TIA, as the calculation results, $\overline{e_T^2}$ is 40 nV²/Hz and $\overline{i_T^2}$ is 3.2 fA²/Hz at 1 kHz, $\overline{e_T^2}$ is 40 nV²/Hz and $\overline{i_T^2}$ is 3.2 fA²/Hz at 10 kHz, and $\overline{e_T^2}$ is 23 nV²/Hz and $\overline{i_T^2}$ is 88 fA²/Hz at 100 kHz. According to the simulation results, the proposed TIA has a bandwidth of over 200 kHz, and the noises of the proposed TIA are lower than the commercial ones with the same transimpedance gain at 1 kHz. This apparatus is very suitable to be equipped in STM for researches of complex organic systems and quality tests of wide bandgap semiconductors in semiconductor industry.

CONFLICT OF INTEREST

The authors declare that they have no conflicts of interest.

REFERENCES

1. Li, Q.F., Wang, Q., Hou, Y.B., and Lu, Q.Y., *Rev. Sci. Instrum.,* 2012, vol. 83, p. 043706. https://doi.org/10.1063/1.3703568
2. Hou, Y.B., Wang, J.H., and Lu, Q.Y., *Rev. Sci. Instrum.,* 2008, vol. 79, p. 113707. https://doi.org/10.1063/1.3005484
3. Ding, Y.Q., Wang, X.Y., Xie, L., Yao, X.Y., and Xu, W., *Chem. Commun.,* 2018, vol. 54, p. 9259. https://doi.org/10.1039/c8cc03585g
4. Im, J.O., Sen, S., Lindsay, S., and Zhang, P.M., *ACS Nano,* 2018, vol. 12, p. 7067. https://doi.org/10.1021/acsnano.8b02819
5. Ding, Y.Q., Xie, L., Yao, X.Y., and Xu, W., *Chem. Commun.,* 2018, vol. 54, p. 3715. https://doi.org/10.1039/c8cc01134f
6. Li, D.L., Sun, L.Y., Ding, Y.Q., Liu, M.X., Xie, L., Liu, Y.F., Shang, L.N., Wu, Y.F., Jiang, H.J., Chi, L.F., Qiu, X.H., and Xu, W., *ACS Nano,* 2021, vol. 15, p. 16896. https://doi.org/10.1021/acsnano.1c07842
7. Zhuang, X.Y., Wu, Q., Zhang, A.H., Liao, L.X., and Fang, B.S., *Chin. J. Chem. Eng.,* 2021, vol. 30, p. 212. https://doi.org/10.1016/j.cjche.2020.10.031
8. Liao, C.C. and Yau, S.L, *Langmuir,* 2022, vol. 38, p. 2495. https://doi.org/10.1021/acs.langmuir.1c02943
9. Carla, M., Lanzi, L., and Pallecchi, E., *Rev. Sci. Instrum.,* 2004, vol. 75, no. 2, p. 497. https://doi.org/10.1063/1.1641159
10. Umbach, C.C. and Blakely, J.M., *Appl. Surf. Sci.,* 2001, vols. 175–176, p. 746. https://doi.org/10.1016/S0169-4332(01)00110-6

11. Data sheet of FEMTO DE-DLPCA-200 Variable Gain Low Noise Current Amplifier. https://www.femto.de/images/pdfdokumente/de-dlpca-200.pdf.; Data Sheet of FEMTO DELCA-200-10G Ultra-Low-Noise Current Amplifier. https://www.femto.de/images/pdfdokumente/de-lca-200-10g.pdf.
12. Data Sheet of OPA657 OPA. https://www.ti.com.cn/cn/lit/ds/symlink/opa657.pdf.
13. Franco, S., *Design with Operational Amplifiers and Analog Integrated Circuits,* McGraw-Hill, 2002.
14. TINA-TI is SPICE-Based Analog Simulation Program Produced by Texas Instruments Inc. https://www.ti.com/tool/TINA-TI.
15. Data Sheet of THS4021 OPA. https://www.ti.com/lit/ds/symlink/ths4021.pdf.
16. Michel, B., Novotny, L., and Dürig, U., *Ultramicroscopy,* 1992, vols. 42–44, p. 1647. https://doi.org/10.1016/0304-3991(92)90499-A
17. Liang, Y.X., *Ultramicroscopy,* 2022, vol. 234, p. 13466. https://doi.org/10.1016/j.ultramic.2022.113466
18. Qian, Z.H., *J. Northeast Norm. Univ., Nat. Sci. Ed.,* 2003, vol. 35, no. 2, p. 41. https://doi.org/10.3321/j.issn:1000-1832.2003.02.008
19. van der Ziel, A., *Noise in Solid State Devices and Circuits,* New York: Wiley-Interscience, 1986.